Journal of
Clinical Medicine

MDPI

Systematic Review

Radiomics in Pituitary Adenomas: A Systematic Review of Clinical Applications and Predictive Models

Edoardo Agosti [1,*], Marcello Mangili [1], Pier Paolo Panciani [1], Lorenzo Ugga [2], Vittorio Rampinelli [3], Marco Ravanelli [4], Alessandro Fiorindi [1] and Marco Maria Fontanella [1,*]

[1] Neurosurgery Unit, Department of Medical and Surgical Specialties, Radiological Sciences and Public Health, University of Brescia, 25123 Brescia, Italy; m.mangili005@studenti.unibs.it (M.M.); pierpaolo.panciani@unibs.it (P.P.P.); alessandro.fiorindi@asst-spedalicivili.it (A.F.)
[2] Department of Advanced Medical and Surgical Sciences, University of Campania "Luigi Vanvitelli", 80131 Naples, Italy; lorenzo.ugga@gmail.com
[3] Unit of Otorhinolaryngology—Head and Neck Surgery, Department of Surgical Specialties, Radiological Sciences, and Public Health, University of Brescia, 25123 Brescia, Italy; vittorio.rampinelli@unibs.it
[4] Radiology Unit, Department of Medical and Surgical Specialties, Radiological Sciences and Public Health, University of Brescia, 25123 Brescia, Italy; marco.ravanelli@unibs.it
* Correspondence: edoardo_agosti@libero.it.com (E.A.); marco.fontanella@unibs.it (M.M.F.)

Abstract

Background: Radiomics offers quantitative, high-dimensional data from conventional imaging and holds promise for improving diagnosis and treatment of pituitary adenomas (PAs). This systematic review aimed to synthesize current clinical applications of radiomics in PAs, focusing on diagnostic, predictive, and prognostic modeling. **Methods**: This review followed the PRISMA 2020 guidelines. A systematic search was performed in PubMed, Scopus, and Web of Science on 10 January 2024, and updated on 5 March 2024, using predefined keywords and MeSH terms. Studies were included if they evaluated radiomics-based models using MRI for diagnosis, classification, consistency, invasiveness, treatment response, or recurrence in human PA populations. Data extraction included study design, sample size, MRI sequences, feature types, machine learning algorithms, and model performance metrics. Study quality was assessed via the Newcastle-Ottawa Scale. Descriptive statistics summarized study characteristics; no meta-analysis was performed due to heterogeneity. **Results**: Out of 341 identified articles, 49 studies met inclusion criteria, encompassing a total of more than 9350 patients. The majority were retrospective (43 studies, 88%). MRI sequences used included T2-weighted imaging (35 studies, 71%), contrast-enhanced T1WI (34 studies, 69%), and T1WI (21 studies, 43%). PyRadiomics was the most common feature extraction tool (20 studies, 41%). Machine learning was employed in 43 studies (88%), predominantly support vector machines (16 studies, 33%), random forests (9 studies, 18%), and logistic regression (9 studies, 18%). Deep learning methods were applied in 17 studies (35%). Regarding diagnostic performance, 22 studies (45%) reported an (AUC) $\geq$0.85 in test datasets. External validation was performed in only 6 studies (12%). Radiomics applications included histological subtype prediction (14 studies, 29%), surgical outcome prediction (13 studies, 27%), invasiveness assessment (7 studies, 15%), tumor consistency evaluation (8 studies, 16%), and response to medical or radiotherapy treatments (3 studies, 6%). One study (2%) addressed automated segmentation and volumetry. **Conclusions**: Radiomics enables high-performance, noninvasive prediction of PA subtypes, consistency, invasiveness, treatment response, and recurrence, with 22 studies (45%) reporting AUC $\geq$0.85. Despite promising results, clinical translation remains limited by methodological heterogeneity, low external validation (6 studies, 12%), and lack of standardization.

Academic Editor: Victor Volovici

Received: 17 July 2025
Revised: 28 August 2025
Accepted: 13 September 2025
Published: 18 September 2025

Citation: Agosti, E.; Mangili, M.; Panciani, P.P.; Ugga, L.; Rampinelli, V.; Ravanelli, M.; Fiorindi, A.; Fontanella, M.M. Radiomics in Pituitary Adenomas: A Systematic Review of Clinical Applications and Predictive Models. *J. Clin. Med.* **2025**, *14*, 6595. https://doi.org/10.3390/jcm14186595

Keywords: radiomics; machine learning; pituitary adenoma; magnetic resonance imaging; systematic review

1. Introduction

Pituitary adenomas (PAs) represent approximately 10–15% of primary intracranial neoplasms [1–3]. While commonly benign, they are clinically significant due to hormone hypersecretion syndromes and their potential to exert mass effects on adjacent anatomical structures. This dual mechanism of impact can severely compromise patient quality of life [1]. Importantly, over 30% of PAs demonstrate invasive behavior, infiltrating the cavernous sinuses (CSs), bony structures, the hypothalamus, or the internal carotid artery, which can complicate both diagnosis and treatment planning [4,5].

Magnetic resonance imaging (MRI) is the primary imaging modality used in the diagnostic work-up of PAs. It plays a crucial role not only in the initial identification and anatomical localization of the lesion, but also in long-term monitoring of tumor progression or recurrence. The strengths of MRI lie in its high-resolution, multiplanar capabilities and superior soft tissue contrast. However, the traditional approach to MRI interpretation is qualitative and dependent on radiologist expertise, leading to potential inter-observer variability and missed subtle findings. The subjective nature of this evaluation has spurred the development of more objective, reproducible tools [6].

Radiomics is a computational technique that extracts a vast array of quantitative features from standard medical imaging, offering a high-dimensional analysis of tumor phenotypes that surpass visual assessment. These features include intensity, texture, shape, and spatial relationships, capturing microstructural heterogeneity and tumor biology [7]. The field has expanded significantly in recent years, particularly when integrated with artificial intelligence (AI) and machine learning (ML). These tools can build predictive models that automatically interpret complex radiomic data, enhancing diagnostic accuracy, prognostication, and treatment personalization [8–11].

Radiomics has already demonstrated utility in various domains relevant to the clinical management of Pas [12]. Studies have shown its potential in differentiating PAs from other sellar and suprasellar lesions, as craniopharyngiomas and Rathke cleft cysts [13,14]. Additionally, radiomics has proven valuable in preoperative histological subtyping [15–28]. For instance, models trained on multiparametric MRI data have accurately distinguished subtypes, such as silent corticotroph adenomas (SCAs) and null cell adenomas (NCAs), entities that may otherwise be clinically silent yet have different prognostic implications [21–24]. Furthermore, PA consistency, a key factor in predicting the ease and success of surgical resection, has been correlated with specific radiomics features [29–34]. Radiomics also aids in evaluating invasiveness, particularly the prediction of CS invasion through features that align with higher Knosp grades [35–41]. Radiomic models have also shown promise in predicting responsiveness to pharmacologic treatments, like somatostatin receptor ligands in patients with acromegaly, and in forecasting the effects of radiotherapy. These predictions allow for more tailored treatment plans and may help avoid ineffective or unnecessary therapies [42,43]. Lastly, radiomics can contribute to the prognostication of recurrence and progression after surgical resection [44–47].

Despite the growing body of literature, no recent systematic review has comprehensively summarized the current applications of radiomics for PAs, the models that have been proposed, and which approaches have shown the most promising performance [48]. Moreover, even if several studies have been published in recent years covering a wide range of applications from histological characterization and invasion prediction to response

assessment and outcome forecasting, these findings often are still fragmented across the literature. Therefore, the present systematic review aims to collect, organize, and analyze these updated data to provide a clear and accessible summary of the state-of-the-art in radiomics for PAs and its applications.

2. Materials and Methods

This systematic review was conducted in accordance with the Preferred Reporting Items for Systematic Reviews and Meta-Analyses (PRISMA) guidelines [49]. Two reviewers (E.A. and M.M.) independently performed a comprehensive search of the PubMed, Scopus, and Web of Science databases. The initial search was conducted on 10 January 2025, with a final update on 5 May 2025. The articles identified through this search were published between 2018 and 2025.

The search strategy utilized a combination of keywords and MeSH terms, including "radiomics," "artificial intelligence," "machine learning," "pituitary adenoma," "pituitary neuroendocrine tumor," "PitNET," "MRI," and "magnetic resonance imaging." Boolean operators (AND/OR) were employed to construct the search query as follows: ("radiomics" OR "machine learning" OR "artificial intelligence") AND ("pituitary adenoma" OR "PitNET" OR "pituitary neuroendocrine tumor") AND ("MRI" OR "magnetic resonance imaging"). Additional relevant studies were identified by manually screening the reference lists of all selected articles.

Studies were eligible for inclusion if they were published in English, involved human subjects, and investigated the application of radiomics (alone or in combination with AI-based methods) for the diagnosis, classification, prediction, or treatment response assessment of PAs using MRI-based features. Both retrospective and prospective original studies were considered. Articles were excluded if they were review articles, editorials, conference abstracts, purely technical or methodological papers without clinical data, or if they involved only phantom or animal models. Studies lacking clearly reported radiomic methodology, outcome measures, or validation procedures were also excluded.

All references were managed using EndNote X9, and duplicate records were removed prior to screening. Two reviewers (E.A. and M.M.) independently screened titles and abstracts for relevance. Full-text screening was then performed on all articles meeting initial inclusion criteria. Discrepancies at any stage were resolved by discussion or consultation with a third reviewer (P.P.P.).

2.1. Data Extraction

Data were extracted systematically from each included article using a pre-defined standardized data collection sheet. Extracted variables included: first author, year of publication, study design, population size, radiomics pipeline (including image acquisition, segmentation, feature extraction, and model development), type of MRI sequences used, clinical endpoint(s) investigated (e.g., differential diagnosis, subtype classification, tumor consistency, invasion, treatment response, or recurrence), and performance metrics (e.g., accuracy, sensitivity, specificity, and area under the curve, i.e., AUC). Additional details were collected on validation methods (internal or external) and the use of AI or ML algorithms.

2.2. Outcomes

The primary objective of this review was to synthesize and characterize the current applications of radiomics in the clinical management of PAs, including diagnostic differentiation, subtype classification, prediction of invasiveness or consistency, treatment response forecasting, and recurrence risk stratification. Secondary outcomes included an evaluation

of the types and performance of models developed, common methodological patterns, and the overall level of validation achieved across studies.

2.3. Radiomics Quality Assessment

A qualitative assessment using the Radiomics Quality Score (RQS) framework was performed with the aim of critically analyzing and comparing the clinical applicability and translational potential of the various radiomic models developed [50]. Evaluation of the included studies was conducted according also to the IBSI compliance checklist to examine their reproducibility and adherence to technical standards [51]. Since many items in the IBSI checklist overlap with those in the RQS checklists, we included only the items relevant to image pre-processing steps (Table 1).

Table 1. Radiomics quality assessment through RQS and IBSI checklists.

Author, Year	Method	RQS (36)	IBSI (%)
Zhang, 2018 [21]	Handcrafted	14	43
Niu, 2018 [35]	Handcrafted	16	43
Kocak, 2018 [42]	Handcrafted	12	86
Staartjes, 2018 [52]	Deep Learning	13	14
Zeynalova, 2019 [29]	Handcrafted	14	86
Ugga, 2019 [15]	Handcrafted	14	71
Fan, 2019 [53]	Handcrafted	16	43
Fan, 2019 [16]	Handcrafted	18	43
Fan, 2019 [54]	Handcrafted	17	43
Qian, 2020 [55]	Deep Learning	10	29
Peng, 2020 [20]	Handcrafted	12	43
Cuocolo, 2020 [30]	Handcrafted	14	71
Machado, 2020 [44]	Handcrafted	10	86
Park, 2020 [26]	Handcrafted	13	100
Zhu, 2020 [31]	Deep Learning	9	29
Chen, 2020 [34]	Handcrafted	14	43
Zhang, 2020 [45]	Handcrafted	11	4
Li, 2021 [24]	Deep Learning	13	71
Liu, 2021 [27]	Handcrafted	14	14
Park, 2021 [43]	Handcrafted	12	71
Wan, 2021 [32]	Handcrafted	12	100
Wang, 2021 [33]	Handcrafted	13	14
Zhang, 2021 [56]	Handcrafted	14	14
Zhang, 2021 [57]	Handcrafted	12	43
Baysal, 2022 [28]	Deep Learning	18	57
Chen, 2022 [46]	Multimodal	13	43
Fang, 2022 [36]	Deep Learning	14	29
Feng, 2022 [41]	Deep Learning	15	29
Kim, 2022 [37]	Deep Learning	14	57
Park, 2022 [38]	Deep Learning	13	57
Rui, 2022 [22]	Handcrafted	17	29
Shu, 2022 [17]	Deep Learning	13	57
Villalonga, 2022 [58]	Handcrafted	13	14
Zhang, 2022 [39]	Handcrafted	14	71
Gargya, 2023 [59]	Deep Learning	10	57
Shen, 2023 [47]	Handcrafted	16	86
Wang, 2023 [25]	Handcrafted	16	57
Wang, 2023 [23]	Handcrafted	15	86
Zhang, 2023 [60]	Handcrafted	16	86

Table 1. *Cont.*

Author, Year	Method	RQS (36)	IBSI (%)
Zhang, 2023 [61]	Deeep Learning	17	14
A, 2024 [19]	Handcrafted	14	57
Behzadi, 2024 [62]	Deep Learning	15	43
Da Mutten, 2024 [63]	Deep Learning	13	43
Fang, 2024 [40]	Deep Learning	14	29
Ishimoto, 2024 [64]	Deep Learning	−2	71
Liu, 2024 [18]	Combined	19	86
Taslicay, 2024 [13]	Handcrafted	14	86
Zhang, 2024 [65]	Handcrafted	15	100
Agosti, 2025 [66]	Handcrafted	15	71

2.4. Risk of Bias Assessment

The quality of the observational studies included in the review was evaluated using the Newcastle-Ottawa Scale (NOS), which assesses studies across three domains: selection, comparability, and outcome assessment (Figure 1).

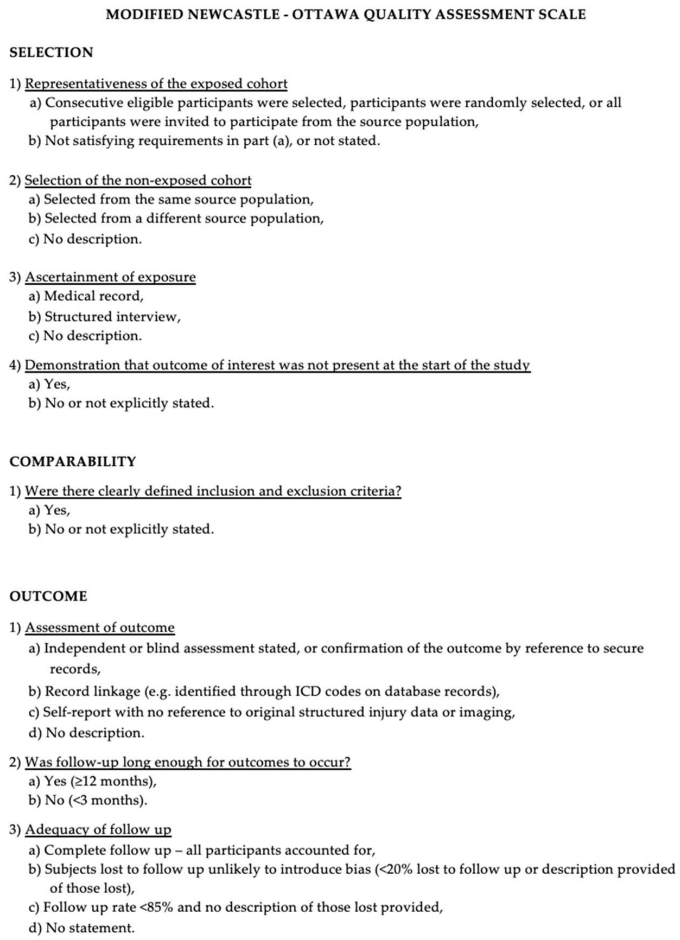

MODIFIED NEWCASTLE - OTTAWA QUALITY ASSESSMENT SCALE

SELECTION

1) Representativeness of the exposed cohort
   a) Consecutive eligible participants were selected, participants were randomly selected, or all participants were invited to participate from the source population,
   b) Not satisfying requirements in part (a), or not stated.

2) Selection of the non-exposed cohort
   a) Selected from the same source population,
   b) Selected from a different source population,
   c) No description.

3) Ascertainment of exposure
   a) Medical record,
   b) Structured interview,
   c) No description.

4) Demonstration that outcome of interest was not present at the start of the study
   a) Yes,
   b) No or not explicitly stated.

COMPARABILITY

1) Were there clearly defined inclusion and exclusion criteria?
   a) Yes,
   b) No or not explicitly stated.

OUTCOME

1) Assessment of outcome
   a) Independent or blind assessment stated, or confirmation of the outcome by reference to secure records,
   b) Record linkage (e.g. identified through ICD codes on database records),
   c) Self-report with no reference to original structured injury data or imaging,
   d) No description.

2) Was follow-up long enough for outcomes to occur?
   a) Yes (≥12 months),
   b) No (<3 months).

3) Adequacy of follow up
   a) Complete follow up – all participants accounted for,
   b) Subjects lost to follow up unlikely to introduce bias (<20% lost to follow up or description provided of those lost),
   c) Follow up rate <85% and no description of those lost provided,
   d) No statement.

Figure 1. Newcastle-Ottawa Scale variables.

Each study could receive a maximum of 9 points. Those scoring below 7 were classified as low quality and excluded from the analysis. Studies that met or exceeded this threshold were retained, and their quality scores were considered during subgroup analyses and narrative synthesis to explore potential sources of bias. A detailed breakdown of NOS scores for each study is available in Table S1.

2.5. Statistical Analysis

Descriptive statistics were used to summarize study characteristics, radiomics applications, and model performance metrics. Results were presented using medians, ranges, and proportions, where appropriate. Due to methodological heterogeneity across studies—including differences in imaging protocols, feature selection methods, and outcome definitions—a formal meta-analysis was not performed. All data processing and visualization were conducted using R statistical software (version 4.2.0) (https://www.r-project.org, accessed on 3 March 2025).

3. Results

3.1. Literature Review

After removing duplicates, 340 articles were identified. Following a review of titles and abstracts, 76 studies were selected for full-text screening. Of the 74 articles assessed for eligibility, 49 met the inclusion criteria and were retained for the final analysis. The remaining 25 studies were excluded based on the following reasons: 10 were systematic reviews or meta-analyses, 9 did not report selected outcomes and 6 were unrelated to the research question. The articles included in the final analysis were published between 2018 and 2025. An overview of the selection process is presented in the PRISMA flowchart (Figure 2). PRISMA checklist is available in Table S2.

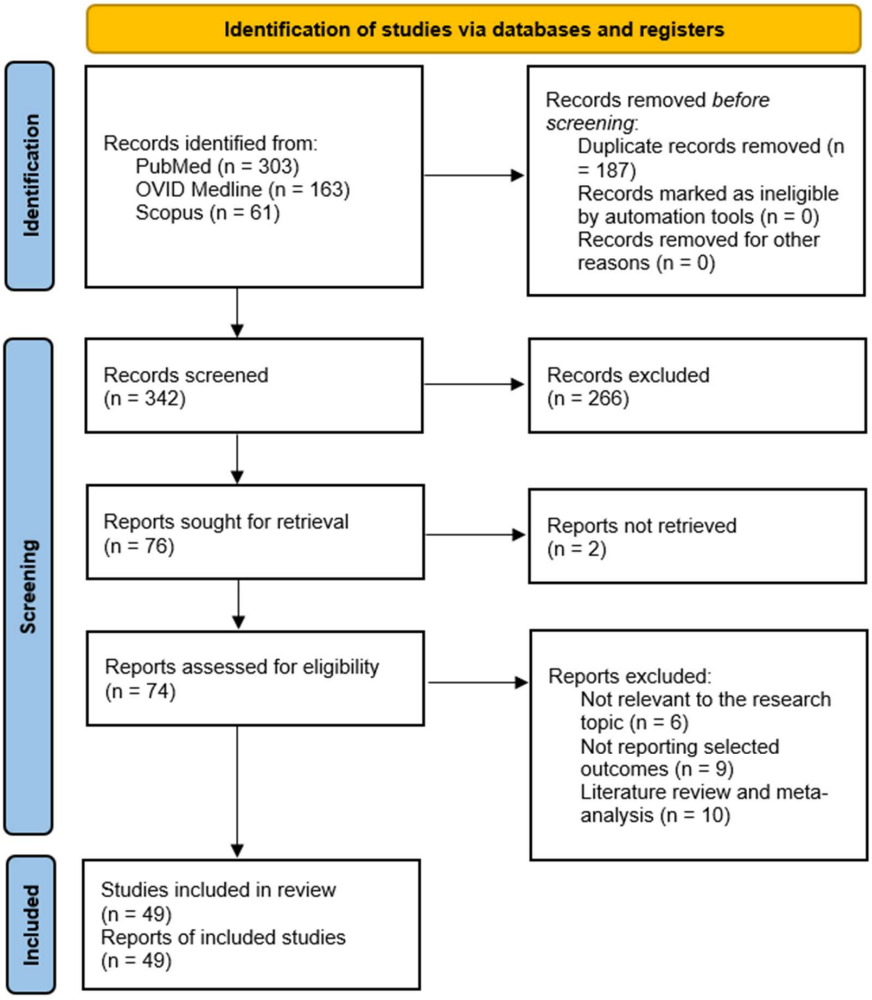

Figure 2. PRISMA flow chart.

3.2. Data Analysis

A total of 49 studies were included in the systematic review, published between 2018 and 2025, investigating the role of radiomics in the assessment and classification of PAs. The total patient population across all studies was approximately 9351, with individual study sample sizes ranging from 24 to 1045 patients. Of these, 30 studies (61%) reported explicit training and test data splits, with 6 studies (12%) including separate validation cohorts. Regarding MRI sequences, were used T1-weighted imaging (T1WI) in 21 studies (43%), T2-weighted imaging (T2WI) in 35 studies (71%), contrast-enhanced T1WI (CE-T1WI) in 34 studies (69%) and T2-weighted imaging FLAIR (T2WI-FLAIR) in 1 study (2%).

In terms of analytical methodology, shallow ML approaches were utilized in 43 studies (88%), while deep learning (DL) architectures were applied in 17 studies (34%), with some studies using both. The most common ML algorithms were support vector machine (SVM) (19 studies, 44%), random forest (RF) (8 studies, 19%), logistic regression (LR) (8 studies, 19%), and k-nearest neighbors (7 studies, 16%). For DL, convolutional neural networks (CNNs) were used in 8 studies (47%), with architectures such as ResNet, DenseNet, and U-net represented. Feature extraction was performed using PyRadiomics in 23 studies (47%), while Matlab-based custom tools were used in 4 studies (8%), and other platforms including 3D Slicer or proprietary scripts in the remaining cases.

The types of radiomic features extracted varied, but first-order statistics (FOS) were used in 18 studies (37%), shape-based features in 20 studies (41%), and texture features (e.g., GLCM, GLRLM, GLSZM, NGTDM, GLDM) in 25 studies (51%). Wavelet-transformed features were included in 10 studies (20%), and higher-order features (e.g., histogram-based or delta-radiomics) were reported in 5 studies (10%).

Regarding tumor subtype, 35 studies (72%) included PAs with any hormonal secretion profile, 7 studies (14%) focused on functional PAs, including GH-secreting, ACTH, TSH, FSH/LH, and prolactinomas, while other 7 (14%) focused on non-functioning PAs (NFPA). The diagnostic performance was reported using AUC or accuracy values in all studies, with AUCs ranging from 0.55 to 1.00. Most models demonstrated high performance, with 22 studies (45%) reporting AUC values $\geq$0.85 in the test set. Further-more, 6 studies (12%) included external validation, strengthening the generalizability of their findings (Table 2).

The most frequently represented field was the prediction of histopathological features, explored in 14 studies (29%), making it the dominant area of investigation. Within this category, the preoperative prediction of Ki-67 index was the most common specific endpoint, analyzed in 5 studies, followed by efforts to distinguish subtypes such as SCAs, NCAs, and Tpit/Pit-1/SF-1 families, and to classify functional versus non-functional adenomas. The second most common field was the prediction of response to surgical treatment, addressed in 13 studies (27%). Of these, post-surgical recurrence or regrowth was the most studied endpoint, featured in 4 studies, indicating its clinical relevance. This was followed by investigations into visual outcome, biochemical remission, and intraoperative cerebrospinal fluid leak prediction. The prediction of tumor consistency and prediction of invasiveness were respectively addressed in 8 and 7 studies (16% and 14%). For consistency, all studies focused on distinguishing soft from fibrous tumors, while the invasiveness category primarily targeted CS invasion (6 studies), and to a lesser extent suprasellar extension. Studies on diagnosis of PAs accounted for 4 publications (8%), with most evaluating automated tumor detection from brain MRI, and one study distinguishing cystic PAs from Rathke's cleft cysts. Lastly, prediction of response to non-surgical treatment, including somatostatin analogs and dopamine agonists (DAs), was investigated in 2 studies (4%), and automated tumor segmentation and volumetry was explored in 1 study (2%) (Table 3).

Table 2. Summary of anamnestic and radiomics data of the studies included in the sys-tematic review. Abbreviations: NF, non-functioning; OC, optic chiasma; ICA, internal ca-rotid artery; GH, growth hormone; IFPA, invasive functional pituitary adenoma; PMA, pi-tuitary macro-adenoma; PRL, prolactin; ACTH, adrenocorticotropic hormone; CPA, cystic pituitary adenoma; RBF-SVM, support vector ma-chine with the radial basis function ker-nel; SVM, support vector machine; MLP, multi-layer perceptron; ANN, artificial neural network; CRNN, convolutional recurrent neural network; kNN, k-nearest neighbors; NB, Naïve Bayes; ET, Extra Trees; RF, Random Forest; LightGBM, light gradient boosting ma-chine; DT, Decision Tree; AdaBoost, Adaptive Boosting; XGBoost, Extreme Gradient Boosting; GBDT, gradient boosting decision tree; BFGS, Broy-den-Fletcher-Goldfarb-Shanno; IF, isolation forest; oSVM, one-class support vector machine; PNN, probabilistic neural network; SNR, signal-to-noise ratio; CNR, con-trast-to-noise ratio; ICA, internal carotid artery; FOS, First Order Statistics; GLCM, Gray Level Gray Level Co-occurrence Matrix; GLRLM, Gray Level Run Length Matrix; GLSZM, Gray Level Size Zone Matrix; NGTDM, Neighboring Gray Tone Difference Matrix; GLDM, Gray Level Dependence Matrix; FOSW, First Order Statistics applied over Wavelet-filtered images; FOSG, First Order Statistics applied over Gradient filtered images; CRNN, Con-volutional Recurrent Neural Network.

Author, Year	Patients				MR Sequences	ML Algorithms Used or AI Model (ML or DL)	Software Used for Features Extraction	Type of Radiomic Features	Tumor Subtype	AUC ROC (or Accuracy %)		
	Total (N)	Training Dataset (%)	Test Dataset (%)	Validation Dataset (%)								
Zhang, 2018 [21]	112	67	33	-	T1WI CE-T1WI	RBF-SVM	MatLab	Intensity Shape and size Texture Wavelet-based	NF	T1WI	Training	0.831
											Test	0.804
										CE-T1WI	Training	0.634
											Test	0.510
Niu, 2018 [35]	194	50	50	-	T2WI CE-T1WI	Linear SVM	MatLab	Intensity Shape and size Texture Wavelet-based ICA wrapped degree	Any		Training	0.852
											Test	0.826
Kocak, 2018 [42]	47	-	-	-	T2WI	kNN C4.5	PyRadiomics (3D-Slicer extension)	FOS GLCM GLRLM GLSZM NGTDM GLDM Wavelet-based	GH	Quantitative TA		0.847
										ROI-based quantitative rSI		0.581
Staartjes, 2018 [52]	140	-	-	-	CE-T1WI	MLP (DL) LR	-	-	Any	MLP (DL)		0.962
										LR		0.86
Zeynalova, 2019 [29]	55	-	-	-	T2WI	ANN	PyRadiomics	-	Any (PMA)	0.710		
Ugga, 2019 [15]	89	60	40	-	T2WI	kNN	PyRadiomics	Shape FOS GLCM GLRLM GLSZM NGTDM GLDM	Any	0.87		

Table 2. *Cont.*

Author, Year	Patients				MR Sequences	ML Algorithms Used or AI Model (ML or DL)	Software Used for Features Extraction	Type of Radiomic Features	Tumor Subtype	AUC ROC (or Accuracy %)		
	Total (N)	Training Dataset (%)	Test Dataset (%)	Validation Dataset (%)								
Fan, 2019 [53]	163	66	34	-	T1WI T2WI CE-T1WI	SVM	Inhouse program written in Matlab 2015b	Intensity Shape and size Texture Wavelet-based	Any (IFPA)	Training		0.832
										Validation		0.811
Fan, 2019 [16]	138	65	35	-	T1WI T2WI CE-T1WI	SVM	PyRadiomics	Shape FOS Texture Wavelet-based	GH	Training		0.96
										Validation		0.89
Fan, 2019 [54]	188	53	31	16	T1WI T2WI CE-T1WI	SVM LR	PyRadiomics	FOS Shape and size GLCM GLRLM GLSZM Wavelet-based	GH	Training		0.83
										Validation		0.81
Qian, 2020 [55]	149	80	20	-	T1WI T2WI	CNN	-	-	Any	-		
Peng, 2020 [20]	235	-	-	-	T1WI T2WI CE-T1WI	SVM kNN NB	PyRadiomics	Shape GLCM GLRLM GLSZM GLDM	Any	SVM	T1WI	0.8762
											T2WI	0.9549
											CE-T1WI	0.8806
										KNN	T1WI	0.8598
											T2WI	0.9266
											CE-T1WI	0.7947
										NB	T1WI	0.8492
											T2WI	0.9324
											CE-T1WI	0.8309
Cuocolo, 2020 [30]	89	80	20	-	T2WI	ET	PyRadiomics	Histogram GLCM GLRLM GLSZM NGTDM GLDM	Any	0.99		

Table 2. *Cont.*

Author, Year	Patients				MR Sequences	ML Algorithms Used or AI Model (ML or DL)	Software Used for Features Extraction	Type of Radiomic Features	Tumor Subtype	AUC ROC (or Accuracy %)		
	Total (N)	Training Dataset (%)	Test Dataset (%)	Validation Dataset (%)								
Machado, 2020 [44]	27	-	-	-	CE-T1WI	kNN RF LR SVM MLP	PyRadiomics	FOS GLCM GLRLM GLSZM NGTDM GLDM FOSW FOSG	NF	MLP		0.929
										RF		0.877
										SVM		0.860
										LR		0.929
										kNN		0.979
Park, 2020 [26]	69	-	-	-	T2WI	-	PyRadiomics	Shape FOS GLCM GLRLM GLSZM NGTDM GLDM	GH	0.834		
Zhu, 2020 [31]	374	-	-	-	T1WI T2WI	-	DenseNet-ResNet based Autoencoder framework CRNN	-	Any	-		
Chen, 2020 [34]	101	71	29	-	T1WI T2WI CE-T1WI	-	-	-	Any	T1WI	Training	0.90
											Test	0.91
										T2WI	Training	0.86
											Test	0.83
										CE-T1WI	Training	0.90
											Test	0.89
										Combined	Training	0.92
											Test	0.91
Zhang, 2020 [45]	50	-	-	-	T2WI CE-T1WI	SVM	Python (v. 3.10.7)	SVR GLCM NGTDM	NF	0.87		
Li, 2021 [24]	185	54	Group 1 24 Group 2 13	9	T1WI T2WI CE-T1WI T2WI-FLAIR	CNN	-	-	Any	Internal Validation 1		0.8063
										Internal validation 2		0.7881
										External independent testing		0.8478

Table 2. *Cont.*

Author, Year	Patients				MR Sequences	ML Algorithms Used or AI Model (ML or DL)	Software Used for Features Extraction	Type of Radiomic Features	Tumor Subtype	AUC ROC (or Accuracy %)		
	Total (N)	Training Dataset (%)	Test Dataset (%)	Validation Dataset (%)								
Liu, 2021 [27]	49	-	-	-	T1WI T2WI CE-T1WI	-	PyRadiomics	Shape FOS GLCM GLRLM GLSZM NGTDM GLDM	GH	ROI1	T1C	0.893
											T1WI	0.918
											T2WI	0.823
											Radiomics	0.908
										ROI2	T1C	0.860
											T1WI	0.898
											T2WI	0.812
											Radiomics	0.880
Park, 2021 [43]	177	80	20	-	T2WI	RF LightGBM ET	PyRadiomics	FOS GLCM GLRLM GLSZM	PRL	Training		0.81
										Test		0.81
Wan, 2021 [32]	156	69	31	-	T1WI T2WI CE-T1WI	RF SVM	MatLab	-	Any (PMA)	0.90		
Wang, 2021 [33]	163	80	20	-	T1WI T2WI CE-T1WI	Linear SVM RF ET kNN DT GDBT AdaBoost MLP XGBoost	PyRadiomics	Knosp grade adenoma volume adenoma diameters OC height ICA contact degree	Any	Linear SVC		0.762
										RF		0.824
										ET		0.865
										KNN		0.920
										DT		0.597
										GBDT		0.807
										AdaBoost		0.817
										MLP		0.856
										XGBoost		0.826
Zhang, 2021 [56]	1045	80	20	-	T1WI T2WI CE-T1WI	GBDT RF AdaBoost XGBoost LR NB DT MLP	-	-	ACTH	XGBoost		0.712
										GBDT		0.734
										RF		0.726
										AdaBoost		0.699
										NB		0.681
										LR		0.701
										DT		0.664
										MLP		0.700
										Stacking		0.743

Table 2. *Cont.*

Author, Year	Patients				MR Sequences	ML Algorithms Used or AI Model (ML or DL)	Software Used for Features Extraction	Type of Radiomic Features	Tumor Subtype	AUC ROC (or Accuracy %)	
	Total (N)	Training Dataset (%)	Test Dataset (%)	Validation Dataset (%)							
Zhang, 2021 [57]	131	-	-	-	T2WI	SVM RF LDA	PyRadiomics	Shape FOS GLCM GLRLM GLSZM NGTDM GLDM	Any	SVM LDA RF	0.824 0.801 0.751
Baysal, 2022 [28]	130	70	15	15	T2WI	ANN (BFGS algorithm)	PyRadiomics	Shape FOS High order features	Any	NF GH PRL ACTH PH FSH-LH TSH	0.87 0.89 0.95 0.94 0.74 0.96 0.95
Chen, 2022 [46]	78	80	-	20	T2WI CE-T1WI	MLP CNN	-	-	NF	CNN MLP Multimodal CNN-MLP	0.84 0.73 0.85
Fang, 2022 [36]	371	-	-	-	CE-T1WI	CNN	-	-		Validation fold 1 Validation fold 2 Validation fold 3 Validation fold 4 Validation fold 5	0.89 0.98 0.89 0.96 0.93
Feng, 2022 [41]	695	-	-	-	CE-T1WI	CNN	-		Any	0.98	
Kim, 2022 [37]	67	-	-	-	CE-T1WI	DL	-	Depth of Invasion Degree of contact with intracavernous ICA	Any	1-mm-slice MR 3-mm-slice MR	0.79 0.61
Park, 2022 [38]	104	-	-	-	CE-T1WI	DL	-	-	Any	Reader 1 Reader 2	1-mm-slice MR 0.91 3-mm-slice MR 0.88 1-mm-slice MR 0.92 3-mm-slice MR 0.87

Table 2. *Cont.*

Author, Year	Patients				MR Sequences	ML Algorithms Used or AI Model (ML or DL)	Software Used for Features Extraction	Type of Radiomic Features	Tumor Subtype	AUC ROC (or Accuracy %)	
	Total (N)	Training Dataset (%)	Test Dataset (%)	Validation Dataset (%)							
Rui, 2022 [22]	302	80	20	-	T1WI T2WI CE-T1WI	LDA SVM RF GBM	PyRadiomics (3D-Slicer extension)	Shape (3D) Shape (2D) FOS GLCM GLRLM GLSZM NGTDM GLDM	NF	Ensemble	0.927
Shu, 2022 [17]	261	80	20	-	T2WI CE-T1WI	DL	U-net neural network	-	Any	CE-T1WI	87.4%,
										T2WI	89.4%
										CE-T1WI + T2WI	89.2%
Villalonga, 2022 [58]	144	80	20	-	T1WI T2WI CE-T1WI	IF local outlier factor oSVM	Python	-	Any	-	
Zhang, 2022 [39]	196	90	-	10	CE-T1WI	SVM	PyRadiomics	FOS Shape (3D) GLCM GLSZM GLRLM NGTDM GLDM	Any		0.86
Gargya, 2023 [59]	-	-	-	-	-	CNN (VGG 16, VGG19, ResNet-50, Inception V3) SVM kNN PNN	-	-	Any	VGG16	89%
										VGG19	91.5%
										Resnet 50	91%
										Inception V3	96%
Shen, 2023 [47]	114	70	30	-	T1WI T2WI CE-T1WI	LR	R software	Shape FOS GLCM GLRLM GLSZM NGTDM Wavelet-based	NF	Clinical + radiomics features	0.929
										Only radiomics features	0.844

Table 2. *Cont.*

Author, Year	Patients				MR Sequences	ML Algorithms Used or AI Model (ML or DL)	Software Used for Features Extraction	Type of Radiomic Features	Tumor Subtype	AUC ROC (or Accuracy %)		
	Total (N)	Training Dataset (%)	Test Dataset (%)	Validation Dataset (%)								
Wang, 2023 [25]	246	78	22	-	CE-T1WI	LR	LIFEx	SHAPE_Volume (mL) SHAPE_Volume (vx) SHAPE_Sphericity SHAPE_Surface area SHAPE_Compacity DISCRETIZED_Q3 DISCRETIZED_Kurtosis GLCM GLRM NGLDM GLZLM	Any	Training		0.916
										Test		0.935
Wang, 2023 [23]	295	88	12	-	T1WI T2WI CE-T1WI	Elasticnet LinearSVC RF ET kNN DT GBDT AdaBoost MLP XGBoost	PyRadiomics	-	NF	LinearSVC	Training	0.931
											Test	0.937
										Elasticnet	Training	0.908
											Test	0.915
										RF	Training	0.848
											Test	0.82
										ET	Training	0.831
											Test	0.845
										KNN	Training	0.836
											Test	0.762
										DT	Training	0.615
											Test	0.622
										GBDT	Training	0.862
											Test	0.819
										AdaBoost	Training	0.667
											Test	0.793
										MLP	Training	0.903
											Test	0.905
										XGBoost	Training	0.879
											Test	0.868
Zhang, 2023 [60]	130	70	30	-	T2WI	Linear SVM	PyRadiomics	Shape Histogram Texture Wavelet-based	Any	Delta-radiomic model	Training	0.821
											Test	0.811
										Combined model	Training	0.841
											Test	0.840
Zhang, 2023 [61]	220	80	20	-	T2WI	CNN	-	-	Any	-		

Table 2. *Cont.*

Author, Year	Patients				MR Sequences	ML Algorithms Used or AI Model (ML or DL)	Software Used for Features Extraction	Type of Radiomic Features	Tumor Subtype	AUC ROC (or Accuracy %)			
	Total (N)	Training Dataset (%)	Test Dataset (%)	Validation Dataset (%)									
A, 2024 [19]	222	67	33	-	T1WI T2WI CE-T1WI	SVM LR RF MLP	PyRadiomics	Shape features FOS GLCM GLRLM GLSZM	Any	Multi-sequence (LR)		Training	0.935
												Test	0.886
												Validation	0.840
									Any	Multi-sequence (MLP)		Training	0.957
												Test	0.913
												Validation	0.758
Behzadi, 2024 [62]	220	70	30	-	T1WI T2WI	CNN	-	-	Any			0.898	
Da Mutten, 2024 [63]	213	91	9	-	CE-T1WI	CNN	-	-	Any	-			
Fang, 2024 [40]	729	89	11	-	CE-T1WI	CNN (ResNet-50)	-	-	Any			0.92	
Ishimoto, 2024 [64]	24	-	-	-	CE-T1WI	DL	-	SNR CNR	Any	-			
Liu, 2024 [18]	247	80	20	-	T1WI T2WI CE-T1WI	LR SVM MLP	PyRadiomics (ML model) ResNet50 (DL model)	FOS Shape Texture	Any	ML model	LR	Training	0.789
												Test	0.547
											SVM	Training	0.904
												Test	0.645
											MLP	Training	0.812
												Test	0.620
										DL model	LR	Training	1.000
												Test	0.808
											SVM	Training	1.000
												Test	0.812
											MLP	Training	1.000
												Test	0.765
										DLR model	LR	Training	1.000
												Test	0.810
											SVM	Training	1.000
												Test	0.810
											MLP	Training	0.994
												Test	0.778

Table 2. *Cont.*

Author, Year	Patients				MR Sequences	ML Algorithms Used or AI Model (ML or DL)	Software Used for Features Extraction	Type of Radiomic Features	Tumor Subtype	AUC ROC (or Accuracy %)		
	Total (N)	Training Dataset (%)	Test Dataset (%)	Validation Dataset (%)								
Taslicay, 2024 [13]	65	-	-	-	T1WI T2WI CE-T1WI	SVM LR LGB	PyRadiomics (3D-slicer)	FOS GLCM GLRLM GLSZM NGTDM GLDM	Any (CPA)	SVM		0.956
										LR		0.956
										LGB		0.951
Zhang, 2024 [65]	152	70	30	-	T1WI T2WI CE-T1WI	SVM	PyRadiomics	FOS Shape (3D) Shape (2D) GLCM GLRLM GLSZM NGTDM GLDM	Any	T1WI	Training	0.784
											Test	0.767
										T2WI	Training	0.724
											Test	0.763
										CE-T1WI	Training	0.822
											Test	0.794
										Multiparametric	Training	0.851
											Test	0.847
Agosti, 2025 [66]	394	80	10	10	T2WI	ET	PyRadiomics	Shape FOS GLCM GLRLM GLSZM NGTDM Wavelet-based	Any			0.59

Table 3. Summary of radiomics applications for PAs. Abbreviations: CI, confidential interval; CS, cavernous sinus; SF, sellar floor; PIT-1, positive pituitary transcription factor 1; ICA, internal carotid artery; NFPA, non-functioning pituitary adenoma; NCA, null cell adenoma; CSF, cerebrospinal fluid; GTR, gross total resection; PMA, pituitary macroadenoma; SA, somatostatin analogues; DA, dopamine agonist; MRI, magnetic resonance imaging; GH, growth hormone; IFPA, invasive functional pituitary adenoma.

General Field of Application	Specific Endpoint	Author, Year
Prediction of consistency	Distinction between soft and fibrous tumors	Zeynalova, 2019 [29] Fan, 2019 [54] Cuocolo, 2020 [30] Zhu, 2020 [31] Chen, 2020 [34] Wan, 2021 [32] Wang, 2021 [33] Agosti, 2025 [66]
Prediction of invasiveness	Prediction of CS invasion	Niu, 2018 [35] Fang, 2022 [36] Kim, 2022 [37] Park, 2022 [38] Zhang, 2022 [39] Fang, 2024 [40]
	Prediction of SF invasion	Feng, 2022 [41]
Prediction of histopathological features	Preoperative prediction of Ki67	Ugga, 2019 [15] Fan, 2019 [16] Shu, 2022 [17]
	Prediction of Ki67 and PIT-1	Liu, 2024 [18]
	Distinction between high-risk and low-risk PitNETs (WHO 2021 classifcation)	A, 2024 [19]
	Distinction among Tpit, Pit-1, and SF-1 subfamilies	Peng, 2020 [20]
	Distinction between NCAs and other NFPA subtypes	Zhang, 2018 [21]
	Distinction between SCAs and other NFPA subtypes	Rui, 2022 [22] Wang, 2023 [23]
	Distinction between functioning and nonfunctioning PAs	Li, 2021 [24]
	Prediction of aggressiveness (Ki-67 $\geq$ 3%, positive p53 staining, high mitotic count)	Wang, 2023 [25]
	Prediction of granulation pattern of GH-secreting PAs	Park, 2020 [26] Liu, 2021 [27]
	Prediction of hormonal secretion patterns	Baysal, 2022 [28]
Prediction of response to surgical treatment	Prediction of post-surgical recurrence or regrowth	Machado, 2020 [44] Zhang, 2020 [45] Chen, 2022 [46] Shen, 2023 [47]
	Prediction of post-surgical visual outcome	Zhang, 2021 [57] Zhang, 2023 [61] Zhang, 2023 [60] Zhang, 2024 [65]
	Prediction of post-surgical biochemical remission	Fan, 2019 [53] Zhang, 2021 [56]
	Prediction of intraoperative CSF leak	Villalonga, 2022 [58] Behzadi, 2024 [62]
	Prediction of the likelihood of GTR	Staartjes, 2018 [52]

Table 3. *Cont.*

General Field of Application	Specific Endpoint	Author, Year
Prediction of response to non-surgical treatment	Prediction of response to SA in GH-secreting PMAs	Kocak, 2018 [42]
	Prediction of response to DAs	Park, 2021 [43]
Diagnose PAs	Detection of pituitary tumors from brain MRI	Qian, 2020 [55] Gargya, 2023 [59] Ishimoto, 2024 [64]
	Distinction between pituitary cystic adenomas and Rathke's cleft cysts	Taslicay, 2024 [13]
Automated tumor segmentation and volumetry	Lesion detection, evaluation of progression of pituitary incidentalomas and detection of residual tumor.	Da Mutten, 2024 [63]

4. Discussion

Radiomics has increasingly established itself as a transformative tool in the neuro-oncological field, enabling the extraction of high-dimensional, quantitative features from conventional imaging modalities. In the context of PAs, its applications have rapidly expanded across multiple domains, from diagnostic differentiation and tumor subtyping to surgical outcome prediction and response assessment. This systematic review analyzed 49 studies, encompassing over 9300 patients. It highlights both the promise and limitations of current radiomics research in this field and offers a framework for future directions.

4.1. Radiomics Quality Assessment

Through RQS evaluation we observed patterns that echo those identified by Kocak et al. [67] in their recent meta-analysis of 1574 radiomics studies across radiological subspecialties. While the number of published works is steadily increasing, the median RQS remains modest (approximately 30%) reflecting persistent gaps in reproducibility, standardization, and clinical readiness.

Some methodological strengths were recurrently observed. Most studies adequately reported imaging protocols, frequently including acquisition parameters such as magnetic field strength, slice thickness, and TR/TE values. Feature reduction strategies to mitigate overfitting were commonly employed, and performance metrics (particularly ROC curves and AUC values) were almost universally reported, establishing a baseline level of analytical rigor. More recently, an encouraging trend has emerged toward multicenter cohorts and external validation, in contrast to earlier works that relied heavily on single-center data and internal validation techniques.

Nonetheless, several critical limitations persist. None of studies included phantom experiments or test–retest imaging, both of which are essential for evaluating feature robustness across scanners and timepoints. Calibration statistics, integral for assessing the clinical reliability of predictive models, were seldom reported. The integration of radiomic features with non-imaging variables, such as clinical, histopathological, or molecular data, was inconsistent, thus limiting the development of comprehensive, biologically informed models. Most notably, very few studies provided access to code, segmentation masks, or extracted feature sets, undermining transparency and reproducibility, issues explicitly highlighted by the IBSI and by Lambin et al. in their foundational framework [50,51].

Validation remains the principal barrier to clinical applicability. Over 90% of the studies reviewed relied exclusively on internal validation methods, with true external validation still rarely implemented. This raises substantial concerns regarding the generalizability of radiomic signatures across centers, scanners, and patient populations. As Kocak et al. [67]

demonstrated, studies employing higher-quality validation strategies consistently achieved superior RQS scores and more reliable results.

This systematic analysis highlights also a marked heterogeneity in adherence to the IBSI preprocessing guidelines, which are crucial for ensuring reproducibility, comparability of extracted features and for enabling clinical translation. Overall, a bimodal distribution emerges: on one side, radiomics-oriented studies, often published in the last five years, present well-defined and transparent pipelines that closely follow IBSI standards; on the other, many deep learning–based works reduce preprocessing to minimal or non-standardized steps. High-quality studies (adherence to checklist >70%), typically report isotropic voxel resampling with explicit target dimensions and sometimes interpolation methods, apply rigorous intensity normalization such as z-score, min–max scaling or sigma-based filtering, include multiscale filters like Laplacian of Gaussian and wavelet with specified parameters, and describe gray-level discretization either through fixed bin width or fixed bin number. They also provide robust ROI processing, often with manual or semi-automatic three-dimensional segmentation validated by interobserver reproducibility measures such as ICC or Dice, and in several cases report artifact correction methods like N4ITK bias field correction. These characteristics are consistently observed in reference studies such as those by Kocak et al. [42], Zeynalova et al. [29], Machado et al. [44], Wan et al. [32], Park et al. [26], Zhang et al. [65], Liu et al. [18], Taslicay et al. [13], Shen et al. [47] Cuocolo et al. [30] and Ugga et al. [15], which stand out for their methodological rigor and reproducibility, allowing replication and multicentric integration. In contrast, low-quality studies in this terms (adherence to the IBSI checklist <30%) omit voxel isotropic resampling and rely on simple resizing or cropping, neglect intensity normalization, do not apply IBSI-compliant filters, and fail to report discretization of gray levels. Segmentation is often absent or replaced with fixed bounding boxes, and no artifact correction is performed, despite the well-known susceptibility of MRI to inhomogeneities. These deficiencies, seen in works such as those by Staartjes et al. [52], Qian et al. [55], Fang et al. [36], Feng et al. [41], Villalonga et al. [58], Liu et al. [27], Wang et al. [33], and Zhang et al. [61], reflect a tendency to prioritize raw CNN learning over methodological transparency, with the consequence that performance metrics obtained in single-center settings cannot be readily generalized. It should be acknowledged that the IBSI compliance checklist, while essential for assessing reproducibility and methodological rigor in traditional handcrafted radiomics, presents inherent limitations when applied to studies employing deep learning techniques, in particular to CNNs. Many IBSI items are specifically designed to evaluate predefined feature extraction and discretization steps, which are not explicitly performed in CNN-based pipelines. As a result, deep learning studies may receive lower IBSI scores, not necessarily due to inferior quality, but because of a methodological mismatch.

4.2. Diagnostic and Subtype Classification

Although the biochemical diagnosis of functioning PAs is relatively straightforward, imaging-based classification remains relevant for differential diagnosis, particularly in the case of silent subtypes or incidentalomas. Numerous studies have explored the use of radiomics in identifying hormonal secretion profiles and tumor subtypes. Baysal et al. [28] demonstrated that artificial neural networks trained on T2WI radiomic features could distinguish seven different hormone-secreting profiles, with AUCs ranging from 0.74 to 0.96, including high performance in distinguishing GH-secreting adenomas (AUC = 0.89) and prolactinomas (AUC = 0.95). Similar subtype classification efforts were conducted by Peng et al. [20], who developed machine learning classifiers (SVM, KNN, NB) capable of distinguishing transcription factor–based PitNET families (Tpit, Pit-1, SF-1) with an AUC up to 0.95 based on multiparametric MRI-derived features.

Specific studies targeted NFPAs, with a focus on histological subtypes like silent corticotroph adenomas (SCAs). Rui et al. [22] and Wang et al. [23] both reported high-performing models for preoperative SCA prediction (AUCs > 0.90), combining radiomic features from T1WI, T2WI, and CE-T1WI sequences with clinical data. Zhang et al. [21] extended this approach to distinguish NCAs, achieving concordance indices up to 0.86 using radiomic nomograms based on T1WI features. Furthermore, in GH-secreting tumors, Park et al. [26] applied radiomics to assess granulation patterns, yielding AUC of 0.83, underscoring radiomics relevance in treatment stratification for acromegaly. A similar model is presented by Liu et al. [27] achieving an AUC of 0.92, with DCA showing that their prediction model had a better net benefit than either the treatment or no treatment schemes when the threshold probability was 0.254 to 0.798.

4.3. Prediction of Tumor Consistency

Preoperative assessment of tumor consistency is vital for surgical planning, as fibrous tumors often pose greater technical challenges during resection. Radiomics has demonstrated utility in this domain, primarily through the analysis of T2WI signal textures. Zeynalova et al. [29] used artificial neural networks to predict tumor consistency with an AUC of 0.71, outperforming conventional signal intensity ratios. Cuocolo et al. [30] further refined this approach using an ensemble learning classifier trained on T2WI-derived features, achieving an AUC of 0.99 and an accuracy of 93%.

Other studies expanded this paradigm to include multiparametric MRI. Wan et al. [32] analyzed T1WI, T2WI, and CE-T1WI sequences using 3D segmentation and showed that texture and wavelet features outperformed shape features in consistency prediction (AUC = 0.90). In GH-secreting adenomas, Fan et al. [54] developed an elastic net-based radiomic model with external validation that reached AUCs of 0.83–0.81 when combined with Knosp grade with DCA confirming its net benefit for preoperative surgical planning. Moreover, they validated the constructed MR radiomics model through a completely independent multicenter prospective validation set, offering robustness among different image acquisition protocols. These findings suggest that tumor consistency, a previously subjective and intraoperative assessment, can now be inferred with reasonable accuracy using non-invasive, preoperative imaging and radiomics.

4.4. Assessment of Invasiveness and Aggressiveness

Cavernous sinus invasion, as graded by the Knosp classification, significantly impacts surgical decision-making. Radiomics provides an opportunity to enhance preoperative prediction of invasiveness, especially in borderline Knosp grades. Niu et al. [35] developed a radiomic-clinical nomogram that integrated CE-T1WI features such as tumor sphericity and internal carotid artery wrapping, yielding an AUC of 0.90. Their DCA demonstrated that at threshold probabilities above 20%, the radiomics nomogram provided greater net benefit compared to conventional clinical-radiological models or treating all/none strategies. Similarly, Zhang et al. [14] analyzed 3D CE-T1WI radiomic features and reported AUCs of 0.86 (training) and 0.73 (validation) for predicting invasiveness.

Radiomics has also been applied to define broader histopathological aggressiveness criteria, including proliferation indices such as Ki-67 and p53. Ugga et al. [15] showed that T2WI-based features could predict high Ki-67 expression with an AUC of 0.87 using a KNN classifier. Wang et al. [25] took a multimodal approach, combining radiomic features and Knosp grade to identify aggressive tumors (AUC = 0.94), while Fan et al. [16] applied similar methods in acromegalic patients, achieving AUCs of 0.96 and 0.89 across training and test cohorts and the DCA demonstrated that both a radiomic signature and derived nomogram had tangible utility in acromegaly management Liu et al. [18] introduced a novel

application of dynamic contrast-enhanced MRI (DCE-MRI) for texture feature extraction. By analyzing pharmacokinetic maps such as Ktrans and Kep, they developed a model that achieved an AUC of 0.96 in distinguishing aggressive from non-aggressive PitNETs. Their DLR model DCA curves demonstrated a strong agreement between predicted and observed outcomes in the internal test set and showed superior clinical benefit in the preoperative prediction of concurrent high Ki-67 expression and PIT-1 positivity, marking an innovative step in functional radiomics.

4.5. Prediction of Surgical Outcomes

A key clinical challenge in PA management is the recurrence or progression of residual tumor post-surgery. Galm et al. [68] showed that preoperative T1WI texture metrics such as pixel intensity could stratify recurrence risk in NFPAs, with lower intensity associated with higher recurrence. Machado et al. [44] reported that KNN and RF classifiers trained on CE-T1WI radiomic features achieved AUCs up to 0.98 and 0.96 for recurrence prediction, with 3D segmentation outperforming 2D approaches. Zhang et al. [45] developed a radiomic score using SVMs and demonstrated its value as an independent prognostic factor (AUC = 0.87). In a broader cohort including all adenoma types, Zhang et al. [60] later compared clinical-pathological and radiomic classifiers, reporting improved predictive accuracy with the inclusion of radiomic features (AUC = 0.84 vs. 0.65); moreover DCA results showed that both their delta-radiomic and combined models achieved superior net benefit compared to clinical variables alone, in both development and independent test cohorts.

Post-surgical hormonal remission has also been evaluated. Fan et al. [53] analyzed over 13,000 CE-T1WI features and built a model with AUCs of 0.83–0.81 across training and test cohorts, significantly outperforming models based on clinical parameters alone. They performed a DCA, revealing clinically meaningful benefit at threshold probabilities >13% in the primary cohort and >25% in the validation cohort. These findings indicate that radiomics can contribute meaningfully to post-operative outcome prediction.

4.6. Prediction of Response to Medical and Radiotherapy

Radiomics is increasingly being evaluated as a tool to predict the efficacy of pharmacologic therapies, particularly in functioning PAs. Kocak et al. [42] applied texture analysis to T2WIs in acromegaly patients and found that radiomic classifiers (KNN) outperformed qualitative and semi-quantitative signal assessments in predicting response to somatostatin receptor ligands (AUC = 0.85). In this study there were significant differences, with the best performances shown by the quantitative texture analysis based radiomic model, in terms of sensitivity, specificity and AUC-ROC. The other radiomic models were the 2D ROI-based quantitative rSI evaluation model and the 3D segmentation-based quantitative rSI evaluation model, that showed questionable performances if compared to qualitative (visual) rSI evaluation and granulation pattern-based evaluation. Galm et al. [68] correlated T1WI texture parameters with IGF-1 normalization, showing an odds ratio of 5.96 for higher pixel intensity after adjusting for clinical covariates.

Park et al. [43] applied ensemble classifiers to predict DAs response in prolactinoma patients, achieving an AUC of 0.81. Importantly, conventional imaging markers such as T2 intensity or cystic changes were not predictive, highlighting the incremental value of radiomics. Fan et al. [69] further extended the application to radiotherapy outcomes, showing that CE-T1WI-based radiomic models (AUC = 0.92) surpassed clinical-only models (AUC = 0.86). The combined model incorporating both radiomic and clinical data achieved an AUC of 0.96, offering a compelling argument for radiomics-guided treatment stratification in post-operative settings.

4.7. Technical and Methodological Considerations

Most of the reviewed studies utilized T1WI, T2WI, and CE-T1WI sequences, with PyRadiomics as the dominant feature extraction tool. Feature types commonly included FOS, shape descriptors, and texture metrics (GLCM, GLRLM, GLSZM), with increasing use of wavelet and higher-order features. Most studies relied on SVMs, RF, and logistic regression models, though DL architectures (e.g., CNNs, ResNet, DenseNet) have become more prevalent in recent years, particularly in larger datasets such as those reported by Zhang et al., Liu et al., and Gargya et al.

Despite high reported accuracies (AUC $\geq$ 0.80 in 81,6% of studies), generalizability remains a concern. Only 6 studies (12%) performed external validation. Moreover, adherence to radiomics quality standards (e.g., IBSI, RQS) was inconsistently reported, and segmentation protocols varied widely. Few studies applied robustness testing or accounted for variability in imaging acquisition.

4.8. Limitations and Future Directions

While current evidence underscores the potential of radiomics to enhance the clinical management of PAs, several limitations hinder its translation into routine practice. Most studies were retrospective and single-center, with substantial heterogeneity in imaging protocols, segmentation methods, feature extraction, and model validation. Only studies by Fan et al. [54] and Li et al. [24] employed external validation, and adherence to radiomics quality standards was inconsistently reported. The absence of standardized pipelines and variability in performance metrics limit reproducibility and comparability. Future research should emphasize prospective, multicenter studies, standardized methodologies, and clinical integration to advance radiomics toward reliable, personalized care in PA management. High-quality research embodies the potential for integration, harmonization, and reproducibility, whereas lower-quality studies, despite innovations in deep learning, often lack the methodological rigor required for reliable translation. The future of the field lies in the convergence of deep learning approaches with IBSI-standardized preprocessing and adherence to best practices outlined in the RQS framework, as reinforced by Kocak et al. [67] and Lambin et al. [50]

5. Conclusions

This systematic review highlights the expanding role of radiomics in the clinical management of PAs, demonstrating high diagnostic performance across applications such as subtype classification, tumor consistency, invasiveness, and treatment outcome prediction. Radiomic models achieved AUC $\geq$0.85 in 45% of studies, primarily using ML and multiparametric MRI. However, clinical adoption remains limited due to methodological heterogeneity, lack of standardized workflows, and scarce external validation (4%). To enable broader translation into the clinical decision-making process, several concrete recommendations should be prioritized: robustness testing through phantom studies, longitudinal imaging, and inter-observer segmentation variability; rigorous validation, with preference for external and multicenter datasets; transparency through the sharing of code, annotations, and feature sets; integrative modeling that combines radiomic, clinical, and molecular data; and an emphasis on clinical applicability, including the use of calibration and decision curve analyses, as well as the design and registration of prospective studies to evaluate radiomic signatures in real-world workflows.

Supplementary Materials: The following supporting information can be downloaded at: https://www.mdpi.com/article/10.3390/jcm14186595/s1, Table S1: This table summarized the NOS scores of each study included in the systematic review; Table S2: PRISMA checklist (Reference [70] are cited in the Supplementary Materials).

Author Contributions: Conceptualization, E.A., M.M., P.P.P., L.U., V.R., M.R., A.F., and M.M.F.; methodology, E.A., M.M., P.P.P., L.U., V.R., M.R., A.F., and M.M.F.; validation, E.A., M.M., P.P.P., L.U., V.R., M.R., A.F., and M.M.F.; formal analysis, E.A., M.M., P.P.P., L.U., V.R., M.R., A.F., and M.M.F.; investi-gation, E.A. and M.M.; resources, E.A., M.M., P.P.P., L.U., V.R., M.R., A.F., and M.M.F.; data curation, E.A., M.M., P.P.P., L.U., V.R., M.R., A.F., and M.M.F.; writing—original draft prepa-ration, E.A., M.M., P.P.P., L.U., V.R., M.R., A.F., and M.M.F.; writing—review and editing, E.A., M.M., P.P.P., L.U., V.R., M.R., A.F., and M.M.F.; visualization, E.A., M.M., P.P.P., L.U., V.R., M.R., A.F., and M.M.F.; supervision, E.A., M.M., P.P.P., L.U., V.R., M.R., A.F., and M.M.F.; project administration, E.A., M.M., P.P.P., L.U., V.R., M.R., A.F., and M.M.F. All authors have read and agreed to the published version of the manuscript.

Funding: This research received no external funding.

Institutional Review Board Statement: Not applicable.

Informed Consent Statement: Not applicable.

Data Availability Statement: Data available in a publicly accessible repository.

Conflicts of Interest: The authors declare no conflict of interest.

Abbreviations

AI = artificial intelligence, AUC = area under the curve, CS = cavernous sinus, CNN = con-volutional neural network, DCE-MRI = dynamic contrast-enhanced magnetic resonance imaging, DL = deep learning, ML = machine learning, FOS = first-order statistics, GLCM = Gray Level Gray Level Co-occurrence Matrix, GLRLM = Gray Level Run Length Matrix, GLSZM = Gray Level Size Zone Matrix, LR = logistic regression, MRI = magnetic resonance imaging, GLDM = Gray Level Dependence Matrix, NCA = null cell adenoma, NFPA = non-functioning pituitary adenoma, NGTDM = Neighboring Gray Tone Difference Matrix, DA = dopamine agonist, PA = pituitary adenoma RF = random forest, SCA = silent cortico-troph adenoma, SVM = support vector machine.

References

1. Melmed, S. Pituitary-Tumor Endocrinopathies. *N. Engl. J. Med.* **2020**, *382*, 937–950. [CrossRef]
2. Ostrom, Q.T.; Price, M.; Neff, C.; Cioffi, G.; Waite, K.A.; Kruchko, C.; Barnholtz-Sloan, J.S. CBTRUS Statistical Report: Primary Brain and Other Central Nervous System Tumors Diagnosed in the United States in 2015–2019. *Neuro Oncol.* **2022**, *24*, v1–v95. [CrossRef]
3. Asa, S.L.; Mete, O.; Perry, A.; Osamura, R.Y. Overview of the 2022 WHO Classification of Pituitary Tumors. *Endocr. Pathol.* **2022**, *33*, 6–26. [CrossRef]
4. Mehta, G.U.; Lonser, R.R. Management of Hormone-Secreting Pituitary Adenomas. *Neuro Oncol.* **2017**, *19*, 762–773. [CrossRef] [PubMed]
5. Raverot, G.; Dantony, E.; Beauvy, J.; Vasiljevic, A.; Mikolasek, S.; Borson-Chazot, F.; Jouanneau, E.; Roy, P.; Trouillas, J. Risk of Recurrence in Pituitary Neuroendocrine Tumors: A Prospective Study Using a Five-Tiered Classification. *J. Clin. Endocrinol. Metab.* **2017**, *102*, 3368–3374. [CrossRef] [PubMed]
6. Molitch, M.E. Diagnosis and Treatment of Pituitary Adenomas: A Review. *JAMA* **2017**, *317*, 516–524. [CrossRef] [PubMed]
7. Scapicchio, C.; Gabelloni, M.; Barucci, A.; Cioni, D.; Saba, L.; Neri, E. A Deep Look into Radiomics. *Radiol. Med.* **2021**, *126*, 1296–1311. [CrossRef]
8. Lambin, P.; Rios-Velazquez, E.; Leijenaar, R.; Carvalho, S.; van Stiphout, R.G.P.M.; Granton, P.; Zegers, C.M.L.; Gillies, R.; Boellard, R.; Dekker, A.; et al. Radiomics: Extracting More Information from Medical Images Using Advanced Feature Analysis. *Eur. J. Cancer* **2012**, *48*, 441–446. [CrossRef]
9. Maniaci, A.; Lavalle, S.; Gagliano, C.; Lentini, M.; Masiello, E.; Parisi, F.; Iannella, G.; Cilia, N.D.; Salerno, V.; Cusumano, G.; et al. The Integration of Radiomics and Artificial Intelligence in Modern Medicine. *Life* **2024**, *14*, 1248. [CrossRef]

10. Gillies, R.J.; Kinahan, P.E.; Hricak, H. Radiomics: Images Are More than Pictures, They Are Data. *Radiology* **2016**, *278*, 563–577. [CrossRef]
11. Ugga, L.; Perillo, T.; Capasso, S.; Negroni, D.; Cuocolo, R. Radiomics in Meningiomas: Pathological and Biomolecular Correlation. In *Meningiomas: From Pathology to Clinics*; Maiuri, F., Del Basso De Caro, M., Eds.; Springer Nature: Cham, Switzerland, 2024; pp. 121–130. ISBN 978-3-031-76680-0.
12. Zheng, B.; Zhao, Z.; Zheng, P.; Liu, Q.; Li, S.; Jiang, X.; Huang, X.; Ye, Y.; Wang, H. The Current State of MRI-Based Radiomics in Pituitary Adenoma: Promising but Challenging. *Front. Endocrinol.* **2024**, *15*, 1426781. [CrossRef] [PubMed]
13. Taslicay, C.A.; Dervisoglu, E.; Ince, O.; Mese, I.; Taslicay, C.; Bayrak, B.Y.; Cabuk, B.; Anik, I.; Ceylan, S.; Anik, Y. A Novel Fusion of Radiomics and Semantic Features: MRI-Based Machine Learning in Distinguishing Pituitary Cystic Adenomas from Rathke's Cleft Cysts. *J. Belg. Soc. Radiol.* **2024**, *108*, 9. [CrossRef] [PubMed]
14. Zhang, Y.; Chen, C.; Tian, Z.; Xu, J. Discrimination between Pituitary Adenoma and Craniopharyngioma Using MRI-Based Image Features and Texture Features. *Jpn. J. Radiol.* **2020**, *38*, 1125–1134. [CrossRef]
15. Ugga, L.; Cuocolo, R.; Solari, D.; Guadagno, E.; D'Amico, A.; Somma, T.; Cappabianca, P.; Del Basso de Caro, M.L.; Cavallo, L.M.; Brunetti, A. Prediction of High Proliferative Index in Pituitary Macroadenomas Using MRI-Based Radiomics and Machine Learning. *Neuroradiology* **2019**, *61*, 1365–1373. [CrossRef] [PubMed]
16. Fan, Y.; Chai, Y.; Li, K.; Fang, H.; Mou, A.; Feng, S.; Feng, M.; Wang, R. Non-Invasive and Real-Time Proliferative Activity Estimation Based on a Quantitative Radiomics Approach for Patients with Acromegaly: A Multicenter Study. *J. Endocrinol. Investig.* **2020**, *43*, 755–765. [CrossRef]
17. Shu, X.-J.; Chang, H.; Wang, Q.; Chen, W.-G.; Zhao, K.; Li, B.-Y.; Sun, G.-C.; Chen, S.-B.; Xu, B.-N. Deep Learning Model-Based Approach for Preoperative Prediction of Ki67 Labeling Index Status in a Noninvasive Way Using Magnetic Resonance Images: A Single-Center Study. *Clin. Neurol. Neurosurg.* **2022**, *219*, 107301. [CrossRef]
18. Liu, F.; Zang, Y.; Feng, L.; Shi, X.; Wu, W.; Liu, X.; Song, Y.; Xu, J.; Gui, S.; Chen, X. Concomitant Prediction of the Ki67 and PIT-1 Expression in Pituitary Adenoma Using Different Radiomics Models. *J. Imaging Inform. Med.* **2024**, *38*, 394–409. [CrossRef]
19. Sathya, A.; Goyal-Honavar, A.; Chacko, A.G.; Jasper, A.; Chacko, G.; Devakumar, D.; Seelam, J.A.; Sasidharan, B.K.; Pavamani, S.P.; Thomas, H.M.T. Is Radiomics a Useful Addition to Magnetic Resonance Imaging in the Preoperative Classification of PitNETs? *Acta Neurochir.* **2024**, *166*, 91. [CrossRef]
20. Peng, A.; Dai, H.; Duan, H.; Chen, Y.; Huang, J.; Zhou, L.; Chen, L. A Machine Learning Model to Precisely Immunohistochemically Classify Pituitary Adenoma Subtypes with Radiomics Based on Preoperative Magnetic Resonance Imaging. *Eur. J. Radiol.* **2020**, *125*, 108892. [CrossRef]
21. Zhang, S.; Song, G.; Zang, Y.; Jia, J.; Wang, C.; Li, C.; Tian, J.; Dong, D.; Zhang, Y. Non-Invasive Radiomics Approach Potentially Predicts Non-Functioning Pituitary Adenomas Subtypes before Surgery. *Eur. Radiol.* **2018**, *28*, 3692–3701. [CrossRef]
22. Rui, W.; Qiao, N.; Wu, Y.; Zhang, Y.; Aili, A.; Zhang, Z.; Ye, H.; Wang, Y.; Zhao, Y.; Yao, Z. Radiomics Analysis Allows for Precise Prediction of Silent Corticotroph Adenoma among Non-Functioning Pituitary Adenomas. *Eur. Radiol.* **2022**, *32*, 1570–1578. [CrossRef]
23. Wang, H.; Chang, J.; Zhang, W.; Fang, Y.; Li, S.; Fan, Y.; Jiang, S.; Yao, Y.; Deng, K.; Lu, L.; et al. Radiomics Model and Clinical Scale for the Preoperative Diagnosis of Silent Corticotroph Adenomas. *J. Endocrinol. Invest.* **2023**, *46*, 1843–1854. [CrossRef]
24. Li, H.; Zhao, Q.; Zhang, Y.; Sai, K.; Xu, L.; Mou, Y.; Xie, Y.; Ren, J.; Jiang, X. Image-Driven Classification of Functioning and Nonfunctioning Pituitary Adenoma by Deep Convolutional Neural Networks. *Comput. Struct. Biotechnol. J.* **2021**, *19*, 3077–3086. [CrossRef]
25. Wang, X.; Dai, Y.; Lin, H.; Cheng, J.; Zhang, Y.; Cao, M.; Zhou, Y. Shape and Texture Analyses Based on Conventional MRI for the Preoperative Prediction of the Aggressiveness of Pituitary Adenomas. *Eur. Radiol.* **2023**, *33*, 3312–3321. [CrossRef]
26. Park, Y.W.; Kang, Y.; Ahn, S.S.; Ku, C.R.; Kim, E.H.; Kim, S.H.; Lee, E.J.; Kim, S.H.; Lee, S.-K. Radiomics Model Predicts Granulation Pattern in Growth Hormone-Secreting Pituitary Adenomas. *Pituitary* **2020**, *23*, 691–700. [CrossRef]
27. Liu, C.-X.; Heng, L.-J.; Han, Y.; Wang, S.-Z.; Yan, L.-F.; Yu, Y.; Ren, J.-L.; Wang, W.; Hu, Y.-C.; Cui, G.-B. Usefulness of the Texture Signatures Based on Multiparametric MRI in Predicting Growth Hormone Pituitary Adenoma Subtypes. *Front. Oncol.* **2021**, *11*, 640375. [CrossRef]
28. Baysal, B.; Eser, M.B.; Dogan, M.B.; Kursun, M.A. Multivariable Diagnostic Prediction Model to Detect Hormone Secretion Profile From T2W MRI Radiomics with Artificial Neural Networks in Pituitary Adenomas. *Medeni. Med. J.* **2022**, *37*, 36–43. [CrossRef] [PubMed]
29. Zeynalova, A.; Kocak, B.; Durmaz, E.S.; Comunoglu, N.; Ozcan, K.; Ozcan, G.; Turk, O.; Tanriover, N.; Kocer, N.; Kizilkilic, O.; et al. Preoperative Evaluation of Tumour Consistency in Pituitary Macroadenomas: A Machine Learning-Based Histogram Analysis on Conventional T2-Weighted MRI. *Neuroradiology* **2019**, *61*, 767–774. [CrossRef] [PubMed]
30. Cuocolo, R.; Ugga, L.; Solari, D.; Corvino, S.; D'Amico, A.; Russo, D.; Cappabianca, P.; Cavallo, L.M.; Elefante, A. Prediction of Pituitary Adenoma Surgical Consistency: Radiomic Data Mining and Machine Learning on T2-Weighted MRI. *Neuroradiology* **2020**, *62*, 1649–1656. [CrossRef] [PubMed]

31. Zhu, H.; Fang, Q.; Huang, Y.; Xu, K. Semi-Supervised Method for Image Texture Classification of Pituitary Tumors via CycleGAN and Optimized Feature Extraction. *BMC Med. Inform. Decis. Mak.* **2020**, *20*, 215. [CrossRef]
32. Wan, T.; Wu, C.; Meng, M.; Liu, T.; Li, C.; Ma, J.; Qin, Z. Radiomic Features on Multiparametric MRI for Preoperative Evaluation of Pituitary Macroadenomas Consistency: Preliminary Findings. *J. Magn. Reson. Imaging* **2022**, *55*, 1491–1503. [CrossRef]
33. Wang, H.; Zhang, W.; Li, S.; Fan, Y.; Feng, M.; Wang, R. Development and Evaluation of Deep Learning-Based Automated Segmentation of Pituitary Adenoma in Clinical Task. *J. Clin. Endocrinol. Metab.* **2021**, *106*, 2535–2546. [CrossRef]
34. Chen, J.M.; Wan, Q.; Zhu, H.Y.; Ge, Y.Q.; Wu, L.L.; Zhai, J.; Ding, Z.M. The value of conventional magnetic resonance imaging based radiomic model in predicting the texture of pituitary macroadenoma. *Zhonghua Yi Xue Za Zhi* **2020**, *100*, 3626–3631. [CrossRef]
35. Niu, J.; Zhang, S.; Ma, S.; Diao, J.; Zhou, W.; Tian, J.; Zang, Y.; Jia, W. Preoperative Prediction of Cavernous Sinus Invasion by Pituitary Adenomas Using a Radiomics Method Based on Magnetic Resonance Images. *Eur. Radiol.* **2019**, *29*, 1625–1634. [CrossRef]
36. Fang, Y.; Wang, H.; Feng, M.; Chen, H.; Zhang, W.; Wei, L.; Pei, Z.; Wang, R.; Wang, S. Application of Convolutional Neural Network in the Diagnosis of Cavernous Sinus Invasion in Pituitary Adenoma. *Front. Oncol.* **2022**, *12*, 835047. [CrossRef]
37. Kim, M.; Kim, H.S.; Park, J.E.; Park, S.Y.; Kim, Y.-H.; Kim, S.J.; Lee, J.; Lebel, M.R. Thin-Slice Pituitary MRI with Deep Learning-Based Reconstruction for Preoperative Prediction of Cavernous Sinus Invasion by Pituitary Adenoma: A Prospective Study. *AJNR Am. J. Neuroradiol.* **2022**, *43*, 280–285. [CrossRef]
38. Park, H.; Nam, Y.K.; Kim, H.S.; Park, J.E.; Lee, D.H.; Lee, J.; Kim, S.; Kim, Y.-H. Deep Learning-Based Image Reconstruction Improves Radiologic Evaluation of Pituitary Axis and Cavernous Sinus Invasion in Pituitary Adenoma. *Eur. J. Radiol.* **2023**, *158*, 110647. [CrossRef] [PubMed]
39. Zhang, C.; Heng, X.; Neng, W.; Chen, H.; Sun, A.; Li, J.; Wang, M. Prediction of High Infiltration Levels in Pituitary Adenoma Using MRI-Based Radiomics and Machine Learning. *Chin. Neurosurg. J.* **2022**, *8*, 21. [CrossRef] [PubMed]
40. Fang, Y.; Wang, H.; Cao, D.; Cai, S.; Qian, C.; Feng, M.; Zhang, W.; Cao, L.; Chen, H.; Wei, L.; et al. Multi-Center Application of a Convolutional Neural Network for Preoperative Detection of Cavernous Sinus Invasion in Pituitary Adenomas. *Neuroradiology* **2024**, *66*, 353–360. [CrossRef] [PubMed]
41. Feng, T.; Fang, Y.; Pei, Z.; Li, Z.; Chen, H.; Hou, P.; Wei, L.; Wang, R.; Wang, S. A Convolutional Neural Network Model for Detecting Sellar Floor Destruction of Pituitary Adenoma on Magnetic Resonance Imaging Scans. *Front. Neurosci.* **2022**, *16*, 900519. [CrossRef]
42. Kocak, B.; Durmaz, E.S.; Kadioglu, P.; Polat Korkmaz, O.; Comunoglu, N.; Tanriover, N.; Kocer, N.; Islak, C.; Kizilkilic, O. Predicting Response to Somatostatin Analogues in Acromegaly: Machine Learning-Based High-Dimensional Quantitative Texture Analysis on T2-Weighted MRI. *Eur. Radiol.* **2019**, *29*, 2731–2739. [CrossRef]
43. Park, Y.W.; Eom, J.; Kim, S.; Kim, H.; Ahn, S.S.; Ku, C.R.; Kim, E.H.; Lee, E.J.; Kim, S.H.; Lee, S.-K. Radiomics With Ensemble Machine Learning Predicts Dopamine Agonist Response in Patients With Prolactinoma. *J. Clin. Endocrinol. Metab.* **2021**, *106*, e3069–e3077. [CrossRef]
44. Machado, L.F.; Elias, P.C.L.; Moreira, A.C.; Dos Santos, A.C.; Murta Junior, L.O. MRI Radiomics for the Prediction of Recurrence in Patients with Clinically Non-Functioning Pituitary Macroadenomas. *Comput. Biol. Med.* **2020**, *124*, 103966. [CrossRef] [PubMed]
45. Zhang, Y.; Ko, C.-C.; Chen, J.-H.; Chang, K.-T.; Chen, T.-Y.; Lim, S.-W.; Tsui, Y.-K.; Su, M.-Y. Radiomics Approach for Prediction of Recurrence in Non-Functioning Pituitary Macroadenomas. *Front. Oncol.* **2020**, *10*, 590083. [CrossRef] [PubMed]
46. Chen, Y.-J.; Hsieh, H.-P.; Hung, K.-C.; Shih, Y.-J.; Lim, S.-W.; Kuo, Y.-T.; Chen, J.-H.; Ko, C.-C. Deep Learning for Prediction of Progression and Recurrence in Nonfunctioning Pituitary Macroadenomas: Combination of Clinical and MRI Features. *Front. Oncol.* **2022**, *12*, 813806. [CrossRef]
47. Shen, C.; Liu, X.; Jin, J.; Han, C.; Wu, L.; Wu, Z.; Su, Z.; Chen, X. A Novel Magnetic Resonance Imaging-Based Radiomics and Clinical Predictive Model for the Regrowth of Postoperative Residual Tumor in Non-Functioning Pituitary Neuroendocrine Tumor. *Medicina* **2023**, *59*, 1525. [CrossRef]
48. Cuocolo, R.; Imbriaco, M. Machine Learning Solutions in Radiology: Does the Emperor Have No Clothes? *Eur. Radiol.* **2021**, *31*, 3783–3785. [CrossRef]
49. Page, M.J.; McKenzie, J.E.; Bossuyt, P.M.; Boutron, I.; Hoffmann, T.C.; Mulrow, C.D.; Shamseer, L.; Tetzlaff, J.M.; Akl, E.A.; Brennan, S.E.; et al. The PRISMA 2020 Statement: An Updated Guideline for Reporting Systematic Reviews. *BMJ* **2021**, *372*, n71. [CrossRef]
50. Lambin, P.; Leijenaar, R.T.H.; Deist, T.M.; Peerlings, J.; de Jong, E.E.C.; van Timmeren, J.; Sanduleanu, S.; Larue, R.T.H.M.; Even, A.J.G.; Jochems, A.; et al. Radiomics: The Bridge between Medical Imaging and Personalized Medicine. *Nat. Rev. Clin. Oncol.* **2017**, *14*, 749–762. [CrossRef]
51. The Image Biomarker Standardization Initiative: Standardized Quantitative Radiomics for High-Throughput Image-Based Phenotyping | Radiology. Available online: https://pubs.rsna.org/doi/10.1148/radiol.2020191145 (accessed on 25 August 2025).

52. Staartjes, V.E.; Serra, C.; Muscas, G.; Maldaner, N.; Akeret, K.; van Niftrik, C.H.B.; Fierstra, J.; Holzmann, D.; Regli, L. Utility of Deep Neural Networks in Predicting Gross-Total Resection after Transsphenoidal Surgery for Pituitary Adenoma: A Pilot Study. *Neurosurg. Focus.* **2018**, *45*, E12. [CrossRef]
53. Fan, Y.; Liu, Z.; Hou, B.; Li, L.; Liu, X.; Liu, Z.; Wang, R.; Lin, Y.; Feng, F.; Tian, J.; et al. Development and Validation of an MRI-Based Radiomic Signature for the Preoperative Prediction of Treatment Response in Patients with Invasive Functional Pituitary Adenoma. *Eur. J. Radiol.* **2019**, *121*, 108647. [CrossRef]
54. Fan, Y.; Hua, M.; Mou, A.; Wu, M.; Liu, X.; Bao, X.; Wang, R.; Feng, M. Preoperative Noninvasive Radiomics Approach Predicts Tumor Consistency in Patients With Acromegaly: Development and Multicenter Prospective Validation. *Front. Endocrinol.* **2019**, *10*, 403. [CrossRef] [PubMed]
55. Qian, Y.; Qiu, Y.; Li, C.-C.; Wang, Z.-Y.; Cao, B.-W.; Huang, H.-X.; Ni, Y.-H.; Chen, L.-L.; Sun, J.-Y. A Novel Diagnostic Method for Pituitary Adenoma Based on Magnetic Resonance Imaging Using a Convolutional Neural Network. *Pituitary* **2020**, *23*, 246–252. [CrossRef] [PubMed]
56. Zhang, W.; Sun, M.; Fan, Y.; Wang, H.; Feng, M.; Zhou, S.; Wang, R. Machine Learning in Preoperative Prediction of Postoperative Immediate Remission of Histology-Positive Cushing's Disease. *Front. Endocrinol.* **2021**, *12*, 635795. [CrossRef] [PubMed]
57. Zhang, Y.; Chen, C.; Huang, W.; Cheng, Y.; Teng, Y.; Zhang, L.; Xu, J. Machine Learning-Based Radiomics of the Optic Chiasm Predict Visual Outcome Following Pituitary Adenoma Surgery. *J. Pers. Med.* **2021**, *11*, 991. [CrossRef]
58. Villalonga, J.F.; Solari, D.; Cuocolo, R.; De Lucia, V.; Ugga, L.; Gragnaniello, C.; Pailler, J.I.; Cervio, A.; Campero, A.; Cavallo, L.M.; et al. Clinical Application of the "Sellar Barrier's Concept" for Predicting Intraoperative CSF Leak in Endoscopic Endonasal Surgery for Pituitary Adenomas with a Machine Learning Analysis. *Front. Surg.* **2022**, *9*, 934721. [CrossRef]
59. Gargya, S.; Jain, S. CAD System Design for Pituitary Tumor Classification Based on Transfer Learning Technique. *Curr. Med. Imaging* **2023**, *20*, E15734056246146. [CrossRef]
60. Zhang, Y.; Zheng, J.; Huang, Z.; Teng, Y.; Chen, C.; Xu, J. Predicting Visual Recovery in Pituitary Adenoma Patients Post-Endoscopic Endonasal Transsphenoidal Surgery: Harnessing Delta-Radiomics of the Optic Chiasm from MRI. *Eur. Radiol.* **2023**, *33*, 7482–7493. [CrossRef]
61. Zhang, Y.; Chen, C.; Huang, W.; Teng, Y.; Shu, X.; Zhao, F.; Xu, J.; Zhang, L. Preoperative Volume of the Optic Chiasm Is an Easily Obtained Predictor for Visual Recovery of Pituitary Adenoma Patients Following Endoscopic Endonasal Transsphenoidal Surgery: A Cohort Study. *Int. J. Surg.* **2023**, *109*, 896–904. [CrossRef]
62. Behzadi, F.; Alhusseini, M.; Yang, S.D.; Mallik, A.K.; Germanwala, A.V. A Predictive Model for Intraoperative Cerebrospinal Fluid Leak During Endonasal Pituitary Adenoma Resection Using a Convolutional Neural Network. *World Neurosurg.* **2024**, *189*, e324–e330. [CrossRef]
63. Da Mutten, R.; Zanier, O.; Ciobanu-Caraus, O.; Voglis, S.; Hugelshofer, M.; Pangalu, A.; Regli, L.; Serra, C.; Staartjes, V.E. Automated Volumetric Assessment of Pituitary Adenoma. *Endocrine* **2024**, *83*, 171–177. [CrossRef]
64. Ishimoto, Y.; Ide, S.; Watanabe, K.; Oyu, K.; Kasai, S.; Umemura, Y.; Sasaki, M.; Nagaya, H.; Tatsuo, S.; Nozaki, A.; et al. Usefulness of Pituitary High-Resolution 3D MRI with Deep-Learning-Based Reconstruction for Perioperative Evaluation of Pituitary Adenomas. *Neuroradiology* **2024**, *66*, 937–945. [CrossRef] [PubMed]
65. Zhang, Y.; Huang, Z.; Zhao, Y.; Xu, J.; Chen, C.; Xu, J. Radiomics Using Multiparametric Magnetic Resonance Imaging to Predict Postoperative Visual Outcomes of Patients with Pituitary Adenoma. *Asian J. Surg.* **2024**, *48*, 166–172. [CrossRef] [PubMed]
66. Agosti, E.; Cuocolo, R.; Mangili, M.; Rampinelli, V.; Veiceschi, P.; Cappelletti, M.; Panciani, P.P.; Piazza, A.; Bove, I.; Solari, D.; et al. Radiomics for Preoperative Assessment of Pituitary Adenoma Consistency with T2-Weighted MRI: A Multicenter Study. *J. Neurol. Surg. Part B Skull Base* **2025**. [CrossRef]
67. Kocak, B.; Keles, A.; Kose, F.; Sendur, A. Quality of Radiomics Research: Comprehensive Analysis of 1574 Unique Publications from 89 Reviews. *Eur. Radiol.* **2025**, *35*, 1980–1992. [CrossRef]
68. Galm, B.P.; Martinez-Salazar, E.L.; Swearingen, B.; Torriani, M.; Klibanski, A.; Bredella, M.A.; Tritos, N.A. MRI Texture Analysis as a Predictor of Tumor Recurrence or Progression in Patients with Clinically Non-Functioning Pituitary Adenomas. *Eur. J. Endocrinol.* **2018**, *179*, 191–198. [CrossRef]
69. Fan, Y.; Jiang, S.; Hua, M.; Feng, S.; Feng, M.; Wang, R. Machine Learning-Based Radiomics Predicts Radiotherapeutic Response in Patients With Acromegaly. *Front. Endocrinol.* **2019**, *10*, 588. [CrossRef]
70. Tricco, A.C.; Lillie, E.; Zarin, W.; O'Brien, K.K.; Colquhoun, H.; Levac, D.; Moher, D.; Peters, M.D.J.; Horsley, T.; Weeks, L.; et al. PRISMA Extension for Scoping Reviews (PRISMAScR): Checklist and Explanation. *Ann. Intern. Med.* **2018**, *169*, 467–473. [CrossRef]